

Thermal conductivity contrast measurement of fused silica exposed to low-energy femtosecond laser pulses

Yves Bellouard^{a)}

Micro- and Nano-Scale Engineering, Mechanical Engineering Department, Eindhoven University of Technology, P.O. Box 513, 5600 MB Eindhoven, The Netherlands

Mark Dugan, Ali A. Said, and Philippe Bado

Translume, Inc., 655, Phoenix Drive, Ann Arbor, Michigan 48108-2201

(Received 30 June 2006; accepted 31 August 2006; published online 18 October 2006)

Femtosecond laser irradiation has various noticeable effects on fused silica. Of particular interest, pulses with energy levels below the ablation threshold can locally increase the refractive index and the material etching selectivity to hydrofluoric acid. The mechanism responsible for these effects is not yet fully understood. In this letter, the authors report on local thermal conductivity mapping of laser-affected zones. It is found that these zones exhibit a lower thermal conductivity at room temperature. © 2006 American Institute of Physics. [DOI: 10.1063/1.2363957]

Femtosecond laser pulses interact in unusual ways with matter. In fused silica ($a\text{-SiO}_2$), various interesting effects of femtosecond laser irradiation have been reported. At energy levels below the ablation threshold, the index of refraction can be locally increased¹ and an increased hydrofluoric acid (HF)-etching selectivity in the laser-exposed regions was reported.^{2,3} Although numerous applications have been demonstrated, the underlying physical mechanism to explain these two effects remains elusive.⁴⁻⁶ Of the various proposed models none have achieved universal acceptance by the scientific community due to a lack of supporting experimental evidence. The present study reports on thermal conductivity property variation in the laser-affected zones.

We focus on the effect of low-energy pulses (20–50 nJ) generated at repetition rates sufficiently low to avoid shot-to-shot heat accumulation.⁷ This energy regime is particularly interesting for writing waveguides.⁸

We used a Ti:sapphire femtosecond laser (Coherent RegA) with 100 fs pulses generated at 250 kHz. The focusing optics consists of a 50 \times objective with a numerical aperture of 0.55. A high purity fused silica substrate (Dynasil@1100) is used. This glass is characterized by an OH content in the range of 600–1000 ppm, a Cl content of 90 ppm, and a total metallic impurities content of 1–2 ppm.

The experimental procedure, consisting of three steps, is outlined in Fig. 1. In a first step, patterns consisting of parallel lines with varying spacing are written at a depth of 400 μm below the surface. The specimen is scanned under the laser beam at a speed of 500 $\mu\text{m}/\text{s}$. These lines span the 15 mm specimen width and are written sequentially so that the scanning is always done in the same direction. In a second step, the specimen is cut down the middle using a diamond saw. The cut surfaces are polished until they become optically transparent.

In a final third step, the cut specimen is analyzed using a scanning thermal microscope (SThM) from the company PSIA. This microscope is an atomic force microscope (AFM) equipped with a cantilever incorporating an embedded thermal probe. As in conventional contact-probe AFM, the SThM cantilever is first brought in contact with the

sample. When scanning the surface, irregularities in its morphology deflect the cantilever. A Z-axis scanner is used to counter this deflection by changing the height of the probe, thus maintaining a constant force to the surface. From the Z scanner information one creates the topography profile of the scanned surface. The temperature of the sample is constantly monitored during the scanning. From this data a thermal map is obtained. We use the probe in conductivity contrast imaging (CCM) (Fig. 1 step 3) to measure local changes in the thermal conductivity and see if it correlates to the laser exposed patterns. A resistive element located on the thermal probe locally heats the substrate to a temperature much higher than room temperature. The energy required to maintain the set temperature is representative of the local thermal conductivity. When the heated probe makes contact with the substrate, heat flows from the probe to the sample, resulting in the cooling of the probe. The closed-loop feedback senses this shift, balances the bridge voltage, and restores the probe's resistance (or temperature) to its preset value, as shown in Fig. 1 step 3. The more current needed to maintain the probe set temperature, the higher the thermal conductivity of the specimen.

The laser-exposed patterns have waveguiding properties that make them easy to locate directly in the AFM. Once located a conductivity contrast image is made for various scan sizes (typically 6 \times 6 μm^2 or smaller). For each scan, a matrix of 256 \times 256 measurement points is obtained. Scan-

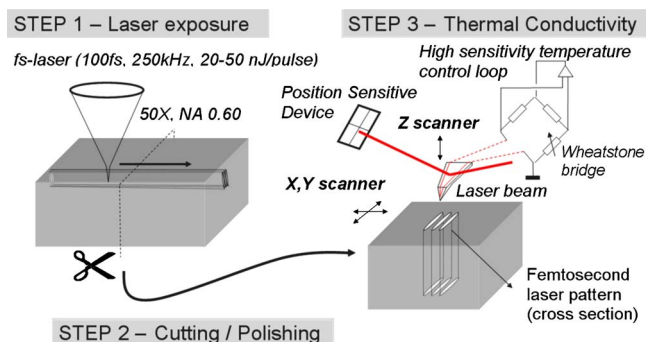


FIG. 1. (Color online) Sample preparation and principle of a scanning thermal microscope used in CCI.

^{a)}Electronic mail: y.bellouard@tue.nl

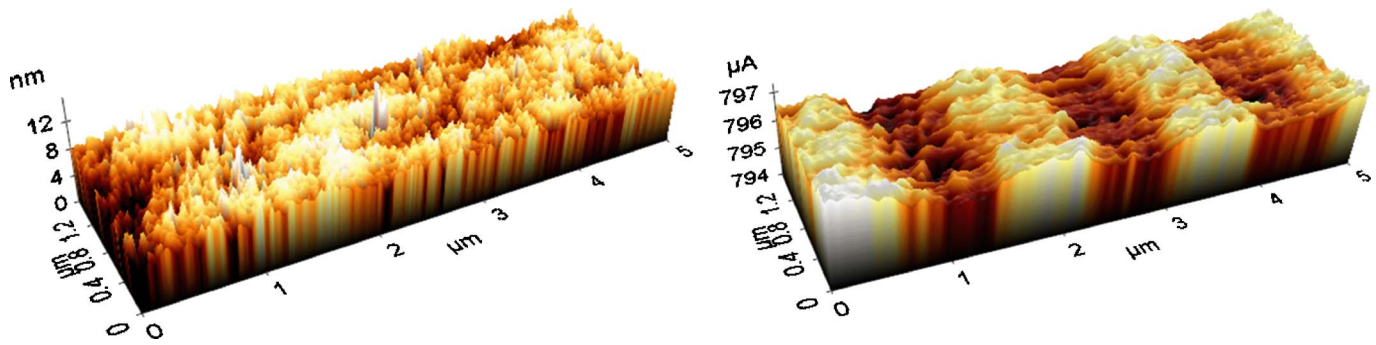


FIG. 2. (Color online) Topography of a portion of laser exposed specimen (left) and corresponding conductivity mapping (right). Spacing between laser tracks is $1.5 \mu\text{m}$ on this specimen.

ning frequency is set to 0.09 Hz to reduce the thermal probe noise level. The set point is chosen in the range of 0.05 to 0.30 nN. Probe currents are set to 0.6 to 0.85 mA depending on surface quality of the region observed.

Figure 2 shows two maps of a zone that has been laser irradiated. On the left we indicate the specimen surface topography, while on the right the corresponding thermal conductivity map is shown. The regions of lower conductivity (darker color) match the position of the laser tracks and correspond to regions of higher refractive index (previously identified with a phase-contrast microscope). Since the topographic map reveals an essentially flat surface with the exception of a surface line defect, variations of thermal conductivity are attributed to structural modification of the material resulting from the laser exposure.

We also explored possible accumulation effects by scanning line patterns multiple times. Considering the compactness of the affected zone (estimated to be 500–700 nm), a perfect overlapping is difficult to achieve in view of the limited accuracy of the positioning stages used to move the specimen under the laser beam. Figure 3 shows an example where after two successive passes some lines are not properly overlapping. Moving from lines 1 to 4 (see Fig. 3), one clearly sees that the overlapping evolves from nearly perfect (line 1) to clearly nonoverlapping (line 4). Figure 4 shows a probe current profile across the conductivity map of Fig. 3.

This example is particularly interesting as it gives some indication about the effect of multiple exposures. Interest-

ingly, no significant difference in terms of probe current intensity is visible between once- and twice-exposed regions. In other words, for the laser parameter used, we do not observe a cumulative effect in the thermal conductivity data.

These experiments show that at low-energy pulses, femtosecond laser irradiation induces a localized decrease of thermal conductivity on fused silica. The zone exhibiting a lower thermal conductivity is typically 500 nm wide and stretched over typically 6–8 μm in the direction of writing laser beam propagation. This pattern matches the zone where higher refractive index⁸ and waveguiding properties are observed. The low thermal conductivity zone is smaller than the laser spot size, which is consistent with the expected nonlinear nature of the femtosecond laser-matter interaction.

Thermal conductivity of fused silica exhibits unusual behavior:⁹ increasing as T^2 at low temperatures, rising to a plateau in the region around $T=10$ K, and then increasing more or less linearly with temperature thereafter. This unusual behavior is related to phonons vibration anomalies whose origins are still subject to discussion and not fully understood.¹⁰ Zhu¹¹ observed experimentally that at room temperature the thermal conductivity of densified fused silica is slightly lower than that of normal fused silica. This suggests that the regions of low thermal conductivity shown on the thermal map have a higher than average density. This interpretation is consistent with a locally increased refractive index as observed in Refs. 1 and 8 and with the hypothesis formulated in Ref. 6 that femtosecond laser irradiation on

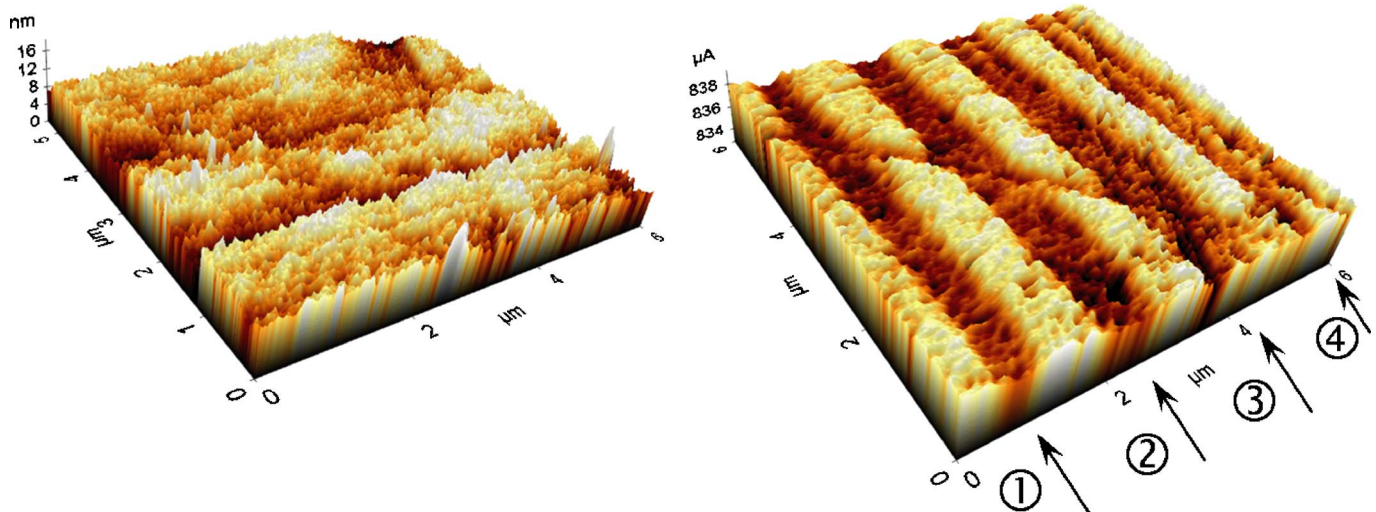


FIG. 3. (Color online) Topography (left) and corresponding conductivity mapping of a specimen scanned multiple times (right).

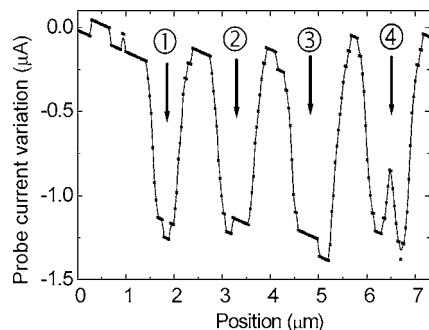


FIG. 4. Average probe current variation across an 8 μm scan of the pattern shown in Fig. 3. Labels indicate track number so that it can easily be matched with Fig. 3.

fused silica induces mostly a localized densification. Other recent observations^{12,13} also point in that direction. Finally, a localized densification is also in accordance with higher HF etching selectivity as reported in Ref. 3 where similar laser parameters were used.

In conclusion, thermal conductivity mapping provides a novel and very capable tool to measure the effects of femtosecond laser irradiation of fused silica. This thermal tool provides higher spatial resolution than traditional optical techniques. Furthermore it requires very little sample preparation.

A lower thermal conductivity at room temperature is observed in the laser-exposed region. Our experimental data coupled with other observations^{3,6,8,12,13} support the case that fused silica is locally densified when exposed to low energy femtosecond pulses.

¹K. M. Davis, K. Miura, N. Sugimoto, and K. Hirao, *Opt. Lett.* **21**, 1729 (1996).

²A. Marcinkevičius, S. Juodkakis, M. Watanabe, M. Miwa, S. Matsuo, H. Misawa, and J. Nishii, *Opt. Lett.* **26**, 277 (2001).

³R. S. Taylor, C. Hnatovsky, E. Simova, D. M. Rayner, M. Mehandale, V. R. Bhardwaj, and P. B. Corkum, *Opt. Express* **11**, 775 (2003).

⁴A. Strelsov and N. Borrelli, *J. Opt. Soc. Am. B* **19**, 2496 (2002).

⁵C. Hnatovsky, R. S. Taylor, E. Simova, P. P. Rajeev, D. M. Rayner, V. R. Bhardwaj, and P. B. Corkum, *Appl. Phys. A* **84**, 47 (2006).

⁶Y. Bellouard, A. Said, M. Dugan, and P. Bado, *Opt. Express* **12**, 2120 (2004).

⁷R. R. Gattass, L. R. Cerami, and E. Mazur, *Opt. Express* **14**, 5279 (2006).

⁸P. Bado, A. Said, M. Dugan, T. Sosnowski, and S. Wright, in *Proceedings of the 18th Annual National Fiber Optic Engineers Conference (NFOEC 2002)*, 15–19 September 2002, Dallas, pp. 1153–1158.

⁹R. C. Zeller and R. O. Pohl, *Phys. Rev. B* **4**, 2029 (1971).

¹⁰E. Courtens, M. Foret, B. Hehlen, and R. Vacher, *Solid State Commun.* **117**, 187 (2001).

¹¹D.-M. Zhu, *Phys. Rev. B* **50**, 6053 (1994).

¹²S. Juodkakis, H. Misawa, T. Hashimoto, E. G. Gamaly, and B. Luther-Davies, *Appl. Phys. Lett.* **88**, 201909 (2006).

¹³Y. Bellouard, T. Colomb, D. Depeursinge, M. Dugan, A. Said, and P. Bado, *Opt. Express* **14**, 8360 (2006).